Molecular Chirality and Charge Transfer through Self-Assembled Scaffold Monolayers

By: J. J. Wei, C. Schafmeister, G. Bird, A. Paul, R. Naaman, and D. H. Waldeck

J. Wei, G. Bird, C. Schafmeister, A. Paul, and D. H. Waldeck, "Molecular chirality and charge transfer through self-assembled scaffold monolayers". *J. of Physical Chemistry B.*; 2006; 110(3); 1301-1308.

Abstract:

The effect of molecular chirality on electron transmission is explored by photoelectrochemistry. Thiol-terminated chiral scaffold molecules containing a porphyrin chromophore were self-assembled on gold surfaces to form a monolayer. Incorporation of the SAM-coated gold into an electrochemical cell and illumination with visible light generated a cathodic photocurrent. When using circularly polarized light, the photocurrent displayed an asymmetry (different magnitude of photocurrent for right versus left polarization) that changed with the molecular chirality (left- or right-handedness of the scaffold). A symmetry constraint on the electronic coupling between the porphyrin and the organic scaffold is proposed as a possible mechanism for the photocurrent asymmetry.

Keywords: photoelectrochemistry | electron transfer | electrochemical cell | cathodic photocurrent

Article:

The primary process of electron transfer underlies many chemical and biological reactions and is of primary importance in many technologies. Consequently, the nature of electron transfer (its dependence on energetics, nuclear degrees of freedom, and electronic coupling) has been under experimental and theoretical study for many years.[1,2] Despite these efforts, little attention has focused on the influence of molecular chirality on electron transfer. This work examines the effect of molecular chirality on the photocurrent of film coated electrodes. On a fundamental level, spin-polarized electrons have been used to perform chemistry and are implicated in the origin of chiral selectivity in biology.[3] On a technological level, molecular chirality can be used to introduce a new control parameter for spin-sensitive devices.

Naaman reported the first investigation of spin dependent electron transmission through thin chiral films of stearoylysine[4] and more recently observed an asymmetry for electron transmission through monolayers of L (or D) polyalanine films.[5] The magnitude of the effect is 10^3 to 10^4 times larger than the chiral selectivity found for the interaction of polarized electrons with molecules that are not organized into two-dimensional arrays.[6-17]

In photoemission through an organic monolayer film, the electron wave function can be delocalized among many chiral molecules in the film, whereas tunneling electrons are more localized. Hence, it is interesting to ask if such large effects are possible for electron tunneling. Spin polarized tunneling has been observed in Metal-Oxide-GaAs (MOS) structures with an asymmetry of the order of 1%.[18] In those studies the polarized distribution of carriers is generated in the GaAs by circularly polarized light and tunneling occurs through a thin Al_2O_3 film (2 to 20 nm) on Al. In recent work spin polarized electrons were selectively transmitted between two quantum dots through an organic molecule.[19] Those findings show that it is possible to create the polarized distribution of charge carriers and observe asymmetry in electron tunneling.

This study investigates the photocurrent, induced by circular polarized light, through organic monolayer films on Au electrodes that are immersed in an electrochemical cell. The films are composed of a chiral scaffold molecule, which is linked to the Au by a cysteine moiety, and presents a porphyrin chromophore to the solution. Although related systems have been studied previously (e.g., Morita et al.[20] placed helical peptides containing a carbazolyl chromophore on gold electrodes), the effects of molecular chirality and light polarization were not explored. Under photoexcitation of the porphyrin, an electron is transferred to an acceptor (e.g., methyl viologen), and the resulting cation of the porphyrin is reduced by the gold electrode. By measuring the dependence of the photocurrent on the polarization of the light field and correlating it with the scaffold's chirality, a preference for electron tunneling of one handedness is indicated.

EXPERIMENTAL SECTION

Reagents and Materials Preparation. Scheme 1 shows the chiral scaffold molecules (L-Cys-(pro4(2S4S))$_4$-Porph (**S1**), D-Cys-(pro4(2R4R))$_4$-Porph (**R1**)) with their covalently linked porphyrin chromophore. The compounds were prepared in the manner reported previously,[21] and details of the synthesis are provided in the Supporting Information.

Solid phase synthesis was performed in a 1.5 mL disposable polypropylene reaction column, connected to a three-way valve equipped with vacuum and argon for mixing. Dichloromethane (DCM) used in coupling reactions was distilled over calcium hydride. Dry grade dimethylformamide (DMF) from Aldrich was used for coupling. Diisopropylamine (DIPEA) was distilled under nitrogen sequentially from ninhydrin and potassium hydroxide and stored over molecular sieves. *O*-(7-Azabenzotriazol-1-yl)-*N*,*N*,*N*‘,*N*‘-tetramethyluronium hexafluorphospate (HATU) was obtained from Acros. All solid-phase reactions were mixed by bubbling argon up through the reactor, allowing for mixing and an inert atmosphere over the reaction. HPLC analysis was performed with a Hewlett-Packard Series 1050 instrument equipped with a Varian Chrompack Microsorb 100 C_{18} column (5 μm packing, 4.6 mm × 250 mm) or a Hewlett-Packard

Series 1100 instrument equipped with a Waters Xterra MS C_{18} column (3.5 μm packing, 4.6 mm × 100 mm) and a diode-array detector.

SCHEME 1

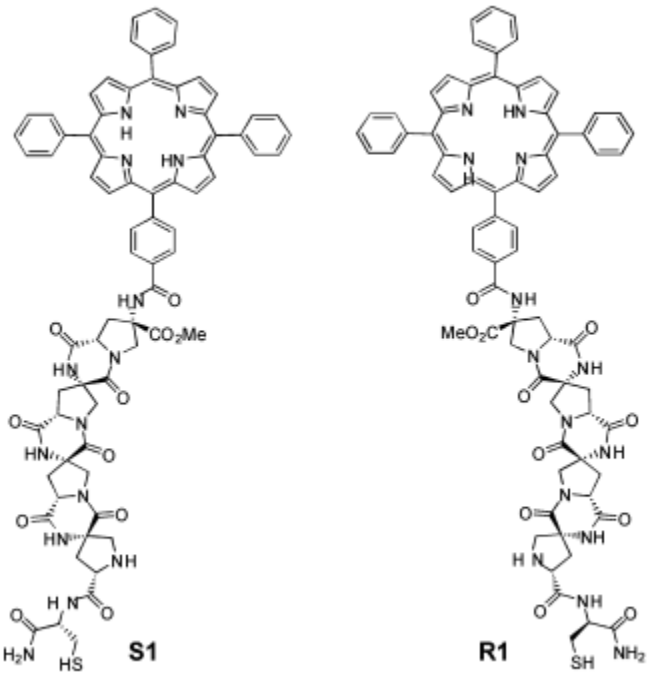

L-Cys-(pro4(2S4S))$_4$-Porph D-Cys-(pro4(2R4R))$_4$-Porph

The HPLC purified product was collected and characterized spectroscopically. The ES-MS displayed a mass-to-charge ratio of 1345.5 for both enantiomers. Circular dichroism spectroscopy was used to characterize the configuration of the scaffold molecules in solution. Room temperature circular dichroism spectra were obtained from a JASCO J-715 spectrometer, using a cell with a 1 cm optical path length.

Film and Electrode Preparation. The molecules were self-assembled to form a monolayer thick film on evaporated gold slides (purchased from EMF Corp.). The Au slides were 0.7 in. × 0.7 in. × 0.062 in. in size and consisted of 100 nm Au on top of a 50 nm thick Ti binder layer on float glass. The gold slides were cleaned by immersion into "piranha" solution (1:3 of H_2O_2 and 98% H_2SO_4) (**Caution: this solution is dangerous**) for a few minutes, then rinsed with a large amount of deionized water (18 MΩ), followed by ethanol, and subsequently dried under an argon gas stream. For adsorption, the molecules were dissolved in a solution with 80%ACN/20%H_2O/0.1%TFA acid at a concentration of about 100 μM. The gold slides were incubated for 1−2 days for pure monolayer preparation at room temperature. These SAM coated gold slides were rinsed with 80%ACN/20%H_2O/0.1%TFA acid solvent before use. To prepare a mixed SAM of the scaffold/porphyrin and an alkanethiol C12 ($HS(CH_2)_{11}CH_3$), the pure scaffold SAM gold slide was immersed in an 80%ACN/20%H_2O/0.1%TFA solution with a 1 mM concentration of C12 alkanethiol for a few (2−6) hours.

Table 1 reports the static contact angles (measured by Gaertner L-117 Null ellipsometer) formed with pure water and the ellipsometrically determined thickness of SAMs composed of the 4-mer chiral scaffold porphyrin SAMs. The SAM coated gold surfaces are more hydrophobic than the bare gold slide's contact angle (60 ± 5°), presumably because of the hydrophobic nature of the terminal porphyrin. No difference in hydrophobicity with the chirality of the scaffold could be detected. The ellipsometric thicknesses for the films, 2.7 ± 0.5 nm for the 4-mer SS and 3.2 ± 0.4 nm for the 4-mer RR scaffold, are less than the length (3.1 nm) of optimized (energy minimized) 4-mer scaffold porphyrins. It was found that the thickness of the scaffold SAM increased if it was incubated in a 1 mM C12 alkanethiol at 80%ACN/20%H_2O/0.1%TFA solution for a few hours. For example, the thickness of a pure 4-mer SS scaffold SAM (2.8 nm) increased to 3.2 nm after 6 h in a 1 mM C12 alkanethiol at 80%ACN/20%H_2O/0.1%TFA solution, and the contact angle of water increased from 80° to 92°. These results suggest that the scaffold molecules may not be compactly assembled at the surface, perhaps because of steric hindrance around the porphyrins.[22]

TABLE 1: Summary of Contact Angle and Thickness of the Scaffold Porphyrin Derivative SAMs at Gold Electrodes[a]

	SAMs of **S1**	SAMs of **R1**
contact angle (deg)	78 ± 5	76 ± 5
thickness (nm)	2.7 ± 0.5	3.2 ± 0.4

[a] Errors are one standard deviation.

The UV−visible absorption spectra of the free porphyrin and the porphyrin scaffolds (**S1** and **R1**) were measured with an Agilent 8435 single beam UV−visible spectrometer. The surface UV−visible absorption spectroscopy was performed by placing a gold coated (200 Å on glass, EMF Corp.) transparent slide in the light beam pathway and measuring the transmission.

Electrochemical Measurements. The compactness of the monolayer films was probed by investigating how well they block faradaic current of a solution redox couple. A CHI180B potentiostat was used for the cyclic voltammetry of electrodes modified with the porphyrin SAMs. The three-electrode cell was composed of a platinum spiral counter electrode, an Ag/AgCl (3 M NaCl) reference electrode, and a porphyrin modified Au slide as a working electrode. The blocking behavior of the SAM modified electrodes was determined in a 0.5 M KCl and 1 mM of $[Fe(CN)_6]^{3-/4-}$ solution.[23] While the bare gold electrode displayed a typical faradaic response, the coated gold electrodes showed a reduced current, which is typical of insulating SAM coated electrodes and indicates that the films inhibit the penetration of the ferricyanide and ferrocyanide redox species to the metal surface (see the Supporting Information). A better blocking behavior was observed from the **R1** coated electrodes than the **S1** coated electrodes, implying a more tightly packed **R1** film than **S1** film.

The porphyrin coverage on the electrodes was estimated by performing cyclic voltammetry in 0.1 M *n*-Bu_4NPF_6 in CH_2ClCH_2Cl or CH_2Cl_2 solution bubbled with argon gas and integrating the area under the faradaic peak to obtain the total charge.

Photocurrent measurements of the porphyrins were performed with a CHI180B potentiostat. The same three-electrode cell was used for the current measurement and the potential applied on the working electrode was controlled. For cathodic photocurrent measurements, the electrochemical

cell contained a 0.1 M Na_2SO_4 aqueous electrolyte solution with 10 mM MV^+ and ambient oxygen as electron acceptors. For anodic photocurrent measurements, a 0.1 M Na_2SO_4, 0.1% TFA aqueous solution with bubbled argon gas was used as an electrolyte solution and contained 50 mM TEOA as an electron donor. For the wavelength-dependent photocurrent measurements, a tungsten−halogen lamp of 25 mW was used as a light source and band-pass filters were used to control the wavelength from 200 to 800 nm. The energy of irradiation was measured by a power/energy meter (Newport Research Corporation (USA), Model 1825C).

For the polarization studies, a He−Cd laser (OmNichrome) source with wavelength 435 nm was used for excitation, by way of a window in the electrochemical cell that was directly opposite the gold slide electrode (see inset of Figure 1). The optical arrangement applied excitation with left/right circular polarized light or linear polarized light through use of a tilted quarter-wave plate (Alphalas Gmbh, Germany) behind a linear polarizer.[24,25] For each measurement, the average power was measured and recorded before and after the photocurrent measurement. Between measurements, the power meter was used to block the light beam. The photocurrent was recorded by a PC through a CHI180B potentiostat.

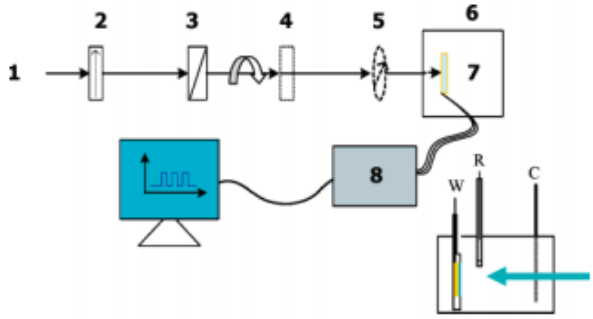

Figure 1. Schematic diagram showing the apparatus for measuring the photocurrent with different light polarization. The components are (1) the He−Cd laser source, (2) a linear polarizer, (3) a tilted quarter wave plate as circular polarizer, (4) a linear polarizer, if needed in the control experiments, (5) an optical power meter, (6) a Faraday cage, (7) an electrochemical cell, and (8) a potentiostat. Number 7 is a three-electrode cell as shown, W is a working electrode, R is the reference electrode, Ag/AgCl, and C is the counter electrode, Pt wire.

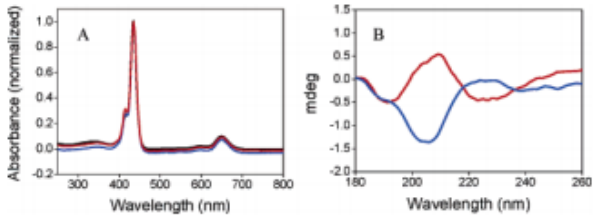

Figure 2. (A) Absorption spectra of porphyrin only (black), **R1** (red), and **S1** (blue) scaffold with porphyrins attached in 80%ACN/20%H_2O/0.1%TFA acid solvent. (B) CD spectra of chiral scaffold molecules: (a) red (**S1**, SS scaffold) and (b) blue (**R1**, RR scaffold). the UV−vis absorbance is normalized to the Soret band.

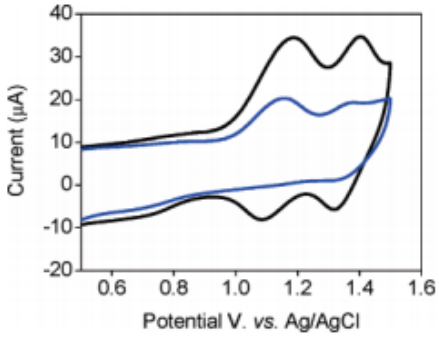

Figure 3. Cyclic voltammograms of the porphyrin scaffold (**R1**) film on a gold slide electrode; the experiment was carried out in *n*-Bu_4NPF_6/CH_2Cl_2 solution with saturated argon gas. The scan rate is 0.4 V/s (black) and 0.2 V/s (blue), Pt is the counter electrode, and Ag/AgCl is the reference electrode.

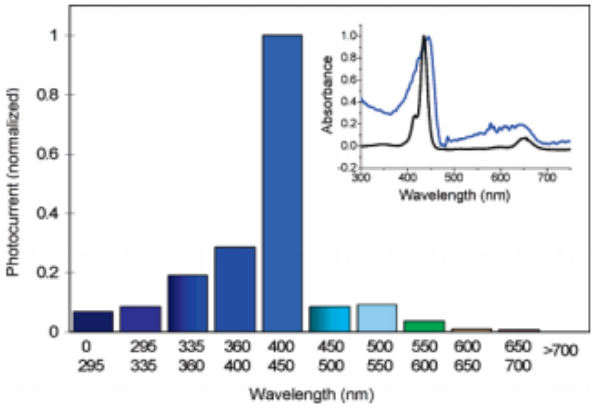

Figure 4. A photocurrent action spectrum; the photocurrent is normalized to the maximum magnitude. The inserted graphic is the UV−visible spectra of scaffold porphyrins (**R1**) in 80%ACN/20%H_2O/0.1%TFA acid solvent (black curve), the scaffold assembled at a gold coated transparent slide in a transmission mode in 80%ACN/20%H_2O/0.1%TFA acid solvent (blue curve). The spectra are normalized to the Soret band absorbance for comparison; the actual absorbance of the surface spectra is about 0.05 at the surface.

RESULTS

Spectra of Scaffold Molecules. Figure 2A shows the absorption spectra of the **S1** and **R1**compounds in 80%ACN/20%H_2O/0.1%TFA acid solution. No significant peak shift is found in the Soret bands (λ_{max} = 435 nm) and Q-bands (649 nm for original porphyrin and 650 nm for scaffold porphyrins) in comparison to the free porphyrin (H_2TPP). This result suggests no significant change of the porphyrin electronic structure in **S1** and **R1**. These results are consistent with previous semiempirical calculations[26] and experiments.[27]

Figure 2B shows CD spectra of the two porphyrin scaffolds in the far-UV region (180−260 nm). It is well-known that the transitions in a polypeptide involve the nonbonding electrons on the oxygen of the carbonyl group and the nearest nitrogen atoms. These transitions are n → π* and π → π*. Normally, the n → π* transition occurs at lower energy and depends on the extent of hydrogen bonding to the oxygen lone pairs, whereas the π → π* transition is dominated by the carbonyl π-bond and occurs at higher energies, ranging from 190 to 210 nm with change in conformation.[28,29]Hence the transition at 225 nm is assigned to the n → π* transitions in the scaffold chain, and the peak centered at 205 nm is assigned to the π → π* transitions.[28,29] The complementary signals of the **R1** and **S1** scaffold reflect the different chirality of these bridges.

Voltammetry of SAMs. Figure 3 shows voltammograms for the porphyrin SAMs that were obtained at a scan rate of 0.4 and 0.2 V/s in a 0.2 M *n*-Bu_4NPF_6/CH_2Cl_2 solution. The porphyrin displays two strong oxidation peaks near 1.12 and 1.36 V vs Ag/AgCl reference electrode at a smaller scan rate (0.2 mV/s). These two oxidation peaks are a characteristic signature for the porphyrin. The lack of reduction peaks at low scan rates arises from the instability of the oxidized porphyrin radicals in the solution.[30] If multiple scans are performed at a slow scan rate the two oxidation peaks become significantly weaker after about 30 min and finally disappear, implying desorption or an inactivity of the resultant scaffold porphyrins. Similar voltammetry was observed from both **S1** and **R1** films (exposure area is 0.3 cm^2).

The surface concentration (electrochemical active species) of porphyrin was estimated by the amount of charge in the first oxidation peak and by the relationship between the peak current and the scan rate.[23] The two methods gave compatible results. Integration of the current peaks provides coverages (after correcting for the surface roughness factor 1.2) of $4.6 \pm 0.2 \times 10^{-11}$mol/$cm^2$ for **S1** and $6.7 \pm 0.15 \times 10^{-11}$ mol/cm^2 for **R1**, almost the same as the coverage of alkane linked porphyrin on ITO[31] and gold electrodes.[32] This coverage is a lower bound, since not all porphyrins at the surface are necessarily electrochemically active, but is consistent with STM images of the film (see the Supporting Information). Assuming that the porphyrin is in a planar conformation and has a circular shape with a 17.0 Å diameter,[32] each porphyrin has an area of about 2.26 nm^2. For a compact porphyrin monolayer, the calculated coverage should be about 7.3×10^{-11} mol/cm^2. These results indicate that the **R1** material has a slightly more compact monolayer structure than the **S1** film (90% versus 60% of a close packed film), consistent with the ellipsometric thickness measurements. The reason for this difference in coverage was not identified.

Action Spectrum of SAMs. The action spectrum of scaffold porphyrins at gold electrodes was obtained by measuring the cathodic photocurrent under irradiation with light, whose wavelength

was selected with band-pass filters. Figure 4 shows the photocurrent action spectrum of an **R1**SAM, and the inset shows its absorbance spectra under different conditions. The greatest photocurrent is observed in the wavelength range of 400 to 450 nm, the Soret band region. The inset shows the spectrum of the porphyrin in 80%ACN/20%H_2O/0.1%TFA acid solvent (black curve), and the spectrum of the **R1** SAM in contact with the 80%ACN/20%H_2O/0.1%TFA acid solvent (blue curve). The films display a broadened Soret band (compared to the solution porphyrin). The photocurrent action spectrum and the absorption spectrum of scaffold porphyrins at the gold surface demonstrate that the porphyrin is the photoactive species responsible for the photocurrent generation.

The broadened Soret band of the porphyrins in the SAMs may have a number of possible origins, such as incomplete protonation of the free tetraphenylporphyrins[26,27] or interactions between porphyrins in the layer, either side-by-side (J aggregation, red shift) or face-to-face (H aggregation, blue shift).[33-36] The Soret band (447) nm of the porphyrin scaffold films in 80%ACN/20%H_2O/0.1%TFA acid solvent is shifted to the red by about 12 nm, and is broadened compared to the spectra in solution. This red shift suggests a strong side-by-side interaction between porphyrins and the broadened peak suggests the presence of both aggregates and porphyrin monomers in the monolayer, which have been reported by others.[37]

Photoelectrochemical Characterization. Photoelectrochemical measurements were performed in a 0.1 M Na_2SO_4 aqueous electrolyte solution containing 10 mM methyl viologen (MV^+) and saturated oxygen as electron acceptors. A cathodic photocurrent from the porphyrin modified gold electrode was observed immediately upon irradiation by a 435 nm laser beam with a power of 1.35 mW at an applied voltage bias of 0.0 V versus Ag/AgCl (3.0 M KCl) reference electrode. A time profile of the raw photocurrent for the **S1** SAM is shown in Figure 5A. The dark current in cathodic photocurrent measurements changes positively with the voltage bias change from 0 to 0.6 V, indicating that the **S1** SAM is not so compact. Nevertheless, the magnitude of the photocurrent was stable, reproducible, and consistent with analogous systems reported earlier.[37]The photocurrent was linear in light intensity for laser powers <3.0 mW. Figure 5B shows the voltage dependence of the photocurrent, which decreases monotonically with increasing positive bias. These results demonstrate that the electron flows from the gold electrode to the electrolyte through the scaffold porphyrin SAMs.

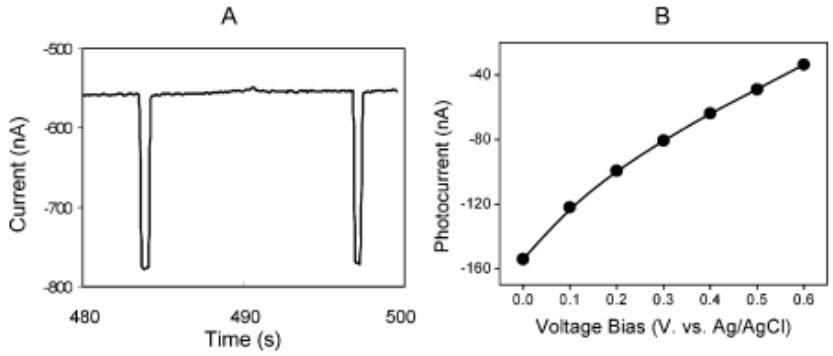

Figure 5. (A) Representative photoelectrochemical responses from the SS scaffold porphyrin SAM modified Au electrode at an applied voltage bias of 0.0 V in a three-electrode cell (counter electrode Pt; reference electrode Ag/AgCl). (B) The voltage bias dependent photocurrents for the Au−porphyrin/$MV^{+/2+}$/Pt system. The excitation wavelength is 435 nm and the average power is 1.35 mW. The photocurrent in panel B is defined as $I_{photo} = I_{on} - I_{off}$.

Similar wavelength responses and voltage dependencies were found for the **R1** and **S1** SAMs at gold electrodes. In addition, no photocurrent was observed from the bare gold electrodes under the irradiation. The photoelectrochemical characterization confirms that excitation of the porphyrin is responsible for photocurrent generation.

Asymmetry of Photocurrent. To study the effect of molecular chirality and electron helicity on the electron transfer, photocurrent generated under irradiation with circularly polarized light (either right circularly polarized light, RCP, or left circularly polarized light, LCP) was examined for both **S1**and **R1** SAMs. Figure 6 shows representative photocurrents generated under illumination with circular polarized light for the two chiral scaffold pophyrins at gold electrodes. The RCP or LCP polarizations were obtained by rotating a λ/4 wave plate at a specific tilt angle (see Experimental Section for details). The incident light intensity was measured for every illumination. For the **S1**scaffold porphyrins, the magnitude of photocurrent under LCP irradiation is slightly larger than that under RCP irradiation as shown in Figure 6A. In contrast, the **R1** scaffold porphyin film has a larger photocurrent under RCP irradiation than that under LCP irradiation. Although the preference is small, less than 1%, it was highly reproducible for a given sample and stable over a period of many hours. In some cases, measurements were performed over more than 1 day on the same electrode and found to be reproducible.

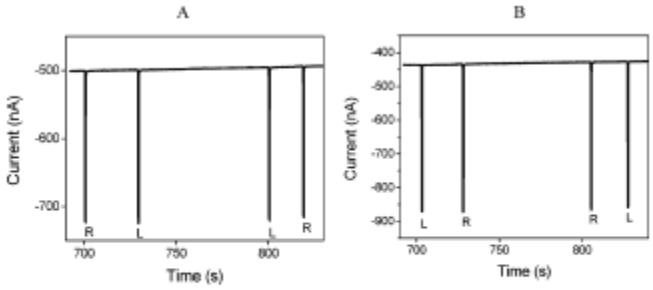

Figure 6. Representative photocurrent signals generated under circular polarized light for (A) **S1** and (B) **R1** scaffold porphyrins at gold electrodes. R and L represent right circularly polarized (RCP) excitation and left circularly polarized excitation (LCP), respectively. The voltage bias is 0.0 V; the incident power is between 1.3 and 1.4 mW.

About 10 electrodes for each sample type (**R1** and **S1**) were studied under the same conditions and the propensities of the asymmetry in photocurrents were measured. Control experiments, using a linearly polarized laser beam, showed no asymmetry.

Asymmetry Factor Determination. An asymmetry factor *A* for the photocurrent was defined as

$$A = \frac{j(\sigma+) - j(\sigma-)}{j(\sigma+) + j(\sigma-)} \qquad (1)$$

in which $j(\sigma+)$ and $j(\sigma-)$ are photocurrents (normalized to light power) for RCP and LCP illumination at the same electrode, respectively. The asymmetry factor was calculated for each RCP and LCP irradiation pair. The **S1** scaffold (4-mer) gave an average asymmetry factor of −0.0048, and the **R1** scaffold (4-mer) gave an average asymmetry factor of +0.0054.

Figure 7 plots the asymmetry factor obtained for all of the experiments. Panels a and b show the distribution (a descending sort) of asymmetry factors for **R1** and **S1** films, respectively. The asymmetry factors of the **R1** scaffold range from −0.017 to 0.034 and most of them are positive values, whereas the asymmetry factors of the **S1** scaffold range from −0.033 to 0.012 and most of them are negative values. Panels c and d show a histogram (bin size of 0.001) for the asymmetry factors. A Gaussian function (solid curve in c and d) is fit to the distribution. This fit yields an average value of 0.004 and a standard deviation of 0.006 for the asymmetry factor of the **R1**scaffold, and it yields an average value of −0.005 and a standard deviation of 0.004 for the **S1**scaffold. This analysis gives an average asymmetry factor of 0.004 ± 0.002 for the **R1** scaffold and −0.005 ± 0.001 for the **S1** scaffold, in which the error in the mean value is the 95% confidence limit.[38]

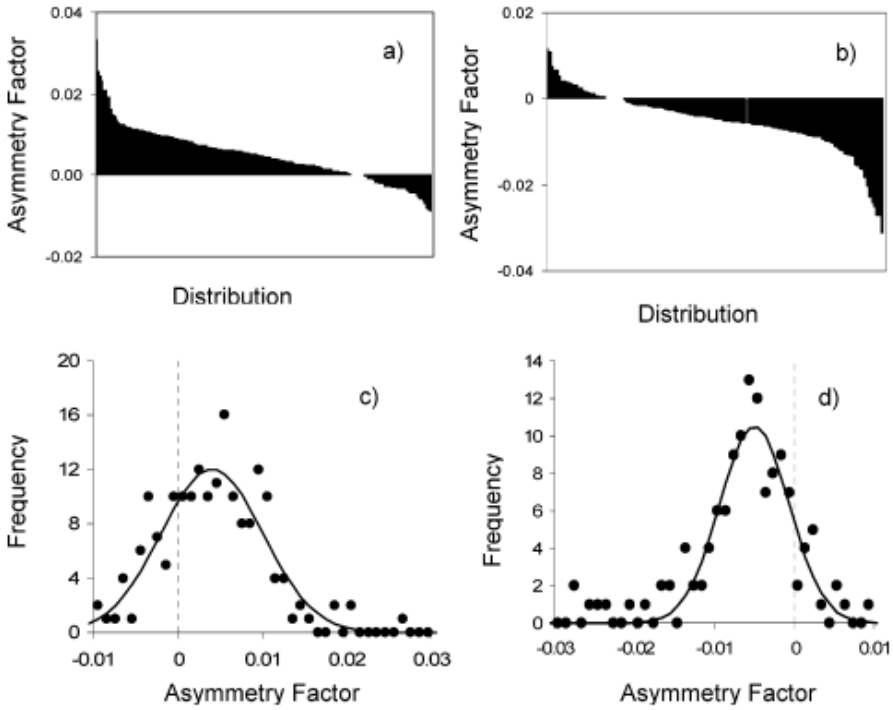

Figure 7. Distributions of asymmetry factors and statistical analysis of the helicities. Panels a and b present the distributions of the asymmetry factors in a descending sort for **R1** and **S1** scaffold porphyrin electrodes, respectively, while panels c and d are the histograms of the number of observations vs the observed ranges of asymmetry factors, corresponding to panels a and b, respectively.

DISCUSSION

Mechanism of Photocurrent Generation and Electron Transfer. The action spectrum (Figure 4) demonstrates that the photocurrent is generated by illumination of the porphyrin Soret band. The mechanism of photocurrent generation from the porphyrin at gold electrodes was established by Imahori et al.,[30,37] and the current findings are consistent with that mechanism.

Figure 8 summarizes the mechanism for cathodic photocurrent generation. Approximating the excited singlet and triplet state energies (relative to the ground state) of porphyrin at the gold surface by their solution values, their redox potentials are estimated to be −0.9 V for $^{1}TPP^{*}/TPP^{+}$and −0.4 V for $^{3}TPP^{*}/TPP^{+}$, using a potential of 1.1 V versus Ag/AgCl for the ground state. In the cathodic photocurrent measurements, the electron acceptors, methyl viologen

(MV^{2+}/MV^{+}) and oxygen (O_2/O_2^{-}), have redox potentials of −0.62 and −0.48 V, respectively. Thus the photoinduced electron transfer only occurs from the excited singlet porphyrin to MV^{2+} and/or O_2. The reduced acceptors, MV^{+} and O_2^{-}, can either reduce the porphyrin cation radicals or diffuse to the Pt counter electrode to generate a cathodic photocurrent. Those cation radicals that do not undergo recombination with the electron acceptors are reduced by electrons from the gold electrode. This phenomenon explains why the magnitude of the cathodic photocurrent depends on the applied voltage.

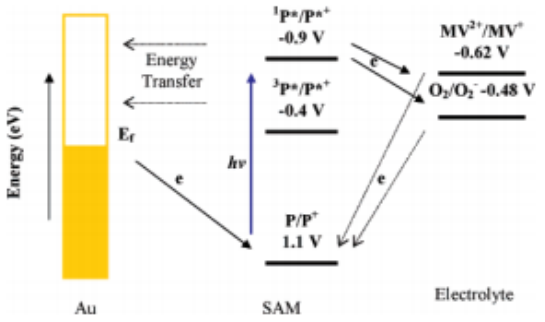

Figure 8. Diagram showing the mechanism for cathodic photocurrent; P represents the porphyrin attached.

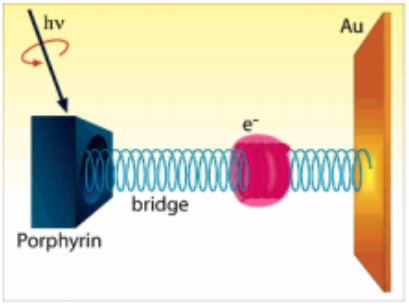

Figure 9. Schematic diagram illustrating the mechanism for photocurrent asymmetry. The light field creates a polarized electron distribution on the porphyrin, and this polarization affects the electron-transfer probability to the electrode because the insulating bridge is chiral.

In addition to the efficiency of charge transfer to the electron acceptor and its subsequent escape, the magnitude of the photocurrent depends on the efficiency of electron tunneling through the scaffold linker[39-41] and energy transfer quenching of the excited singlet porphyrin, by the metal electrode or nearby porphyrin.[30,37] Previous studies of H_2TPP, in both various organic solvents[42,43] and surfaces,[37,44,45] indicate that the lifetime of the excited singlet state of H_2TPP is tens of picoseconds when linked by an alkanethiol to the metal surface, compared to 10 ns in bulk solvents. The lifetime of excited singlet electrons may play an important role, not only in the photocurrent generation, but also in the relative importance of the interaction between the "helicity" of the porphyrin excited state and the scaffold's chirality. In particular, the fast population relaxation of the porphyrin means that the photocurrent arises from short-lived excited states that may retain significant polarization from the exciting light field. Possible mechanisms for the photocurrent's dependence on the electron helicity relative to the bridge chirality are discussed below.

Mechanism for Asymmetry. The mechanism for photocurrent generation does not explain the mechanism for the photocurrent asymmetry. Because the asymmetry is measured for a particular film coated electrode, be it composed of an **R** or an **S** bridge, variations in the film coverage and compactness between the bridge types alone cannot explain the asymmetry. Even though the SS film is more open than the RR film, the asymmetry factors are similar in magnitude (although shifted in sign) implying that defects in the film or access to the metal surface by the viologen is not important for the asymmetry. In addition, linear polarization studies reveal no asymmetry, which implies that the orientational distribution of the chromophores on the surface is isotropic in the plane of the layer (at least on the large length scale probed by the excitation light), implying that geometric/steric constraints on the access to porphyrin moieties do not determine the asymmetry. Two possible explanations are proposed for the asymmetry: (1) dependence of

the tunneling probability on wave function symmetries and (2) induced circular dichroism from packing in the layer.

(*1*) *Electronic Helicities of Excited Porphyrins.* If a molecule is electronically excited by absorption of a photon, the molecules angular momentum changes because the photon carries angular momentum.[46] The transfer of the light field's circular polarization to the ensemble of excited molecules is well established, e.g., circular polarized molecular fluorescence[47,48] and circular dichroism spectroscopy. Other work has demonstrated the generation of electron spin polarization by circularly polarized light in photoemission at surfaces,[49] electron scattering from molecules in the gas phase,[50,51] and other fundamental studies.[52-54] In this work, the asymmetry of photocurrent, generated by irradiation of porphyrin chromophores with circular polarized light, could arise from electron transfer (electron tunneling) that depends on the charge carrier (electron or hole) polarization. Figure 9 illustrates the essential idea that the circularly polarized light excites the porphyrin molecule, promoting an electron to the LUMO with given handedness, or polarization. Hence, an electron with the same handedness can be transferred from the gold substrate to fill the hole in the porphyrin HOMO. When the electron handedness and the chirality of the bridge match, the electron transfer is more efficient.

Electron helicity can be defined as:

$$C = 0.5\,\frac{\sum_l P(m_{l+})}{\sum_l P(m_{l+}) + \sum_l P(m_{l-})} + 0.5\,\frac{P(m_{S+})}{P(m_{S+}) + P(m_{S-})} \quad (2)$$

in which $P(m_{l+})$ and $P(m_{l-})$ are the population in the m_l angular momentum states with positive sign or negative sign, respectively, and $P(m_{S+})$ and $P(m_{S-})$ are the populations of spin $^1/_2$ and spin $-^1/_2$states, respectively. If the spin−orbit coupling is significant, the relevant populations are of the states m_{j+} and m_{j-}, related to j states ($j = l + s$) with positive or negative sign, respectively. For the free porphyrin, the spin−orbit coupling is not expected to be so important.

When the porphyrin is excited with circular polarized light, the orbital that is depopulated, hole, is polarized and its polarization, characterized by an m_l state $|m_l\rangle$, depends on the circular polarization of the photon. The probability that the photogenerated hole is filled by a tunneling electron will depend on the symmetry of the electron wave function. When the electron tunnels through a chiral bridge, the chiral structure of the bridge ensures that certain electron helicities tunnel more efficiently than others, hence the electron wave is polarized and characterized by certain electron helicity, *C*. In the absence of spin−orbit coupling, the electron wave can be described as $\Phi = \sum_l a_l|m'_l\rangle$ in which the coefficients a_l for the $|m'_l\rangle$ states depend on the handedness of the bridge. In the idealized case the left-handed bridge will only transmit m'_l of one sign, and a right-handed bridge the opposite sign. The probability for an electron to be transferred from the metal to the hole state on the acceptor depends on the overlap, *F*, between the hole state and Φ. Therefore, $F = \langle m_l|\Phi\rangle = \langle m_l|\sum_l a_l m'_l\rangle$. For the currently studied case, the axis of quantization is not the same for the two subsystems (chiral bridge and porphyrin ring) and therefore one must account for the projection of $|m_l\rangle$ on the axis of the chiral bridge.

The above considerations should apply if one assumes that spin−orbit coupling is negligible in this system. In the case that it cannot be ignored, one has to consider $j = l + s$ as the valid quantum number.

(*2*) *Circular Dichroism in the Film*. Although the Soret bands (B bands) for the **S1** and **R1**porphyrins do not display a CD signal in solution, their arrangement in a close packed film could induce a dichroism. The broadened and red shifted Soret band suggests a side-by-side interaction between porphyrins in the film. In porphyrin dimers, an exciton interaction can split the B bands and they display circular dichroism. Because of the different chirality of the scaffolds, the porphyrin−porphyrin interaction may have a different "sense" that arises from the geometry of packing, giving rise to a circular dichrosim. This kind of induced electronic "helicity" has been reported from porphyrin assemblies on DNA,[55-57] a helical cyanine dye J-aggregate induced by DNA templates,[58] and other chiral induced systems.[59,60]

If environmentally induced dichroism of the porphyrin Soret band occurs in the SAM film, then the differential absorption of the circularly polarized exciting light could give rise to differential excited-state populations. This dichroism could then give rise to the asymmetry in the photocurrent measurements. Circular dichroism spectra of the monolayer films of **R1** and **S1** were collected. No significant CD signal was observed. The maximum possible asymmetry was calculated to be less than 1 part in 10^4; below the asymmetry observed in the photocurrent experiment, 5 parts in 10^3.

An important caveat to consider is that a different propensity for photocurrent generation could exist for the aggregates of different helicity. In particular, the access of the viologen to the chromophore could be different in the two cases so that the asymmetry one observes in a photocurrent measurement is enhanced over that one may find in an absorption measurement. The fact that the **R** and **S** films had similar asymmetries, while having somewhat different coverage, discounts this explanation somewhat.

CONCLUSIONS

Porphyrins on chiral scaffolds have been assembled on gold electrodes, and the effects of molecular chirality and light helicity on the photocurrent generation have been studied. The photocurrent displays an asymmetry when the chiral monolayer is irradiated by left and right circularly polarized light. The average asymmetry factor obtained for a right-handed monolayer is 0.004 ± 0.002 and that for a left-handed monolayer is -0.005 ± 0.001, with confidence limits of 95%. Experimental and theoretical studies on the coupling of electron helicity and molecular chirality in the gas phase have shown asymmetry factors to be 10^{-3}–10^{-4} for oriented molecules and 10^{-4}–10^{-5} for unoriented molecules.[61-64] The asymmetry factors obtained in this work with the oriented chiral chain are 1 order of magnitude greater than those found from electron scattering[7,8]in the gas phase but less than that of the photoemission through chiral Langmuir−Blodgett assemblies.[5]

The explanation proposed for the phenomenon is that the magnitude of the superexchange coupling through the chiral scaffold depends on the orbital polarization of the excited porphyrin; hence the tunneling probability depends on the light polarization. The relaxation of the orbital

polarization should affect the importance of electron helicity on the coupling to the chiral bridge. If the orbital polarization relaxes rapidly, the nonequilibrium distribution will become depolarized and the influence of molecular chirality will be weak. In the limit of fast relaxation, the value of asymmetry factors would be small. To better understand the mechanism of the observation, further theoretical and experimental work is needed.

ACKNOWLEDGMENT

D.H.W. and C.S. acknowledge support from the U.S. National Science Foundation (CHE-0415457 and CHE-0348823 respectively). D.H.W. and R.N. acknowledge support from the U.S.−Israel Binational Science Foundation. J.W. acknowledges support from a Mellon Fellowship.

Supporting Information Available: Full description of the material preparation, sample STM image, and other characterizations. This material is available free of charge via the Internet at http://pubs.acs.org.

REFERENCES AND NOTES

1. Jortner, J.; Bixon, M., Eds. *Electron-Transfer from Isolated Molecules to Biomolecules*; Advances in Chemical Physics, Vols. 106 and 107; Wiley: New York, 1999.
2. Kuznetsov, A. M. *Charge Transfer in Physics, Chemistry and Biology*; Gordon & Breach: New York, 1995.
3. Avalos, M.; Babiano, R.; Cintas, P.; Jiménez, J. L.; Palacios, J. C.; Barron, L. D. *Chem. Rev.* **1998**, *98*, 2391.
4. Ray, K.; Ananthavel, S. P.; Waldeck, D. H.; Naaman, R. *Science* **1999**, *283*, 814.
5. Carmeli, I.; Skakalova, V.; Naaman, R.; Vager, Z. *Angew. Chem., Int. Ed.* **2002**, *41*, 761.
6. Bonner, W. A. *Chirality* **2000**, *12*, 114 and references therein.
7. Nolting, C.; Mayer, S.; Kessler, J. *J. Phys. B*: *At. Mol. Opt. Phys.* **1997**, *30*, 5491.
8. Mayer, S.; Nolting, C.; Kessler, J. *J. Phys. B* **1996**, *29*, 3497.
9. Mayer, S.; Kessler, J. *Phys. Rev. Lett.* **1995**, *74*, 4803.
10. Beerlage, M. J. M.; Farago, P. S.; Vanderwiel, M. J. *J. Phys. B*: *At. Mol. Opt. Phys*. **1981**, *14*, 3245.
11. Hegstrom, R. A.; Rein, D. W.; Sandars, P. G. H. *J. Chem. Phys.* **1980**, *73*, 2329.
12. Ulbricht, T. L. V.; Vester, F. *Tetrahedron* **1962**, *18*, 629.
13. Bonner, W. A.; Van Dort, M. A.; Yearian, M. R. *Nature* **1975**, *258*, 419.
14. Blum, K.; Thompson, D. G. *Adv. At., Mol. Opt. Phys.* **1997**, *38*, 39.
15. Johnston, C.; Blum, K.; Thompson, D. *J. Phys. B*: *At. Mol. Opt. Phys.* **1993**, *26*, 965.
16. Thompson, D. G.; Kinnin, M. *J. Phys. B*: *At. Mol. Opt. Phys.* **1995**, *28*, 2473;
17. Smith, I. M.; Thompson, D. G.; Blum, K. *J. Phys. B*: *At. Mol. Opt. Phys*. **1998**, *31*, 4029.
18. Prins, M. W. J.; van Kempen, H.; de Groot, R. A.; van Roy, W.; De Boeck, J. *J. Phys. Condens. Matter* **1995**,*7*, 9447.
19. Ouyang, M.; Awschalom, D. D. *Science* **2003**, *301*, 1074.
20. Morita, T.; Kimura, S.; Kobayashi, S.; Imanishi, Y. *J. Am. Chem. Soc.* **2000**, *122*, 2850.

21. Levins, C. G.; Schafmeister, C. E. T. *J. Am. Chem. Soc.* **2003**, *125*, 4702.
22. Imahori, H.; Norieda, H.; Ozawa, S.; Ushida, K.; Yamada, H.; Azuma, T.; Tamaki, K.; Sakata, Y. *Langmuir***1998**, *14*, 5335.
23. Wei, J. J.; Liu, H. Y.; Dick, A. R.; Yamamoto, H.; He, Y. F.; Waldeck, D. H. *J. Am. Chem. Soc.* **2002**, *124*, 9591.
24. Hecht, E. *Optics*, 2nd ed.; Addison-Wesley Publishing Co.: Reading, MA, 1987.
25. Yariv, A.; Yeh, P. *Optical Waves in Crystals;* John Wiley and Sons: New York, 1984.
26. Vitasovic, M.; Gouterman, M.; Linschitz, H. *J. Porphyrins Phthalocyanines* **2001**, *5*, 191.
27. Wasbotten, I. H.; Conradie, J.; Ghosh, A. *J. Phys. Chem. B* **2003**, *107*, 3613.
28. Rodger, A.; Norden, B. *Circular Dichroism and Linear Dichroism*; Oxford University Press: Oxford, UK, 1997; Chapters 2 and 6.
29. Fasman, G. D., Ed. *Circular Dichroism and The Conformational Analysis of Biomolecules*; Plenum: New York, 1996.
30. Yamada, H.; Imahori, H.; Nishimura, Y.; Yamazaki, I.; Ahn, T. K.; Kim, S. K.; Kim, D.; Fukuzumi, S. *J. Am. Chem. Soc.* **2002**, *124*, 9129.
31. Hasobe, T.; Imahori, H.; Yamada, H.; Sato, T.; Ohkubo, K.; Fukuzumi, S. *Nano Lett.* **2003**, *3*, 409.
32. Boeckl, M. S.; Bramblett, A. L.; Hauch, K. D.; Sasaki, T.; Ratner, B. D.; Rogers, J. W., Jr. *Langmuir* **2000**, *16*,5644.
33. Akins, D. L.; Özçelik, S.; Zhu, H.-R.; Guo, C. *J. Phys. Chem.* **1996**, *100*, 14390.
34. Maiti, N. C.; Mazumdar, S.; Periasamy, N. *J. Phys. Chem. B* **1998**, *102*, 1528.
35. Khairutdinov, R. F.; Serpone, N. *J. Phys. Chem. B* **1999**, *103*, 761.
36. Osuka, A.; Maruyama, K. *J. Am. Chem. Soc.* **1988**, *110*, 4454.
37. Imahori, H.; Norieda, H.; Nishimura, Y.; Yamazaki, I.; Higuchi, K.; Kato, N.; Motohiro, T.; Yamada, H.; Tamaki, K.; Arimura, M.; Sakata, Y. *J. Phys. Chem. B* **2000**, *104*, 1253.
38. Taylor, J. R. *An Introduction to* Error *Analysis*, 2nd ed.; University Science Books: Sausalito, CA, 1997.
39. Wei, J. J.; Liu, H. Y.; Khoshtariya, D. E.; Yamamoto, H.; Dick, A.; Waldeck, D. H. *Angew. Chem., Int. Ed.***2002**, *41*, 4700.
40. Khoshtariya, D. E.; Wei, J. J.; Liu, H. J.; Yue, H.; Waldeck, D. H. *J. Am. Chem. Soc.* **2003**, *125*, 7704.
41. Napper, A. M.; Liu, H. Y.; Waldeck, D. H. *J. Phys. Chem. B* **2001**, *105*, 7699.
42. Chirvony, V. S.; Hoek, A.; Galievsky, V. A.; Sazanovich, I. V.; Schaafsma, T. J.; Holten, D. *J. Phys. Chem. B***2000**, *104*, 9909.
43. Gentemann, S.; Medforth, C. J.; Forsyth, T. P.; Nurco, D. J.; Smith, K. M.; Fajer, J.; Holten, D. *J. Am. Chem. Soc.* **1994**, *116*, 7363.
44. Dick, H. A.; Bolton, J. R.; Picard, G.; Munger, G.; Leblanc, R. M. *Langmuir* **1988**, *4*, 133.
45. Imahori, H.; Norieda, H.; Yamada, H.; Nishimura, Y.; Yamazaki, I.; Sakata, Y.; Fukuzumi, S. *J. Am. Chem. Soc.* **2001**, *123*, 100.
46. Meier, F.; Zakharchenya, B. P. *Optical Orientation*: *Modern Problems in Condensed Matter Sciences;* North-Holland: Amsterdam, The Netherlands, 1984; Vol. 8.
47. Green, A. S.; Gallup, G. A.; Rosenberry, M. A.; Gay, T. J. *Phys. Rev. Lett.* **2004**, *92*, 093201.

48. Fiederling, R.; Keim, M.; Reiscjer, G.; Ossau, W.; Schmidt, G.; Waag, A.; Molenkamp, L. W. *Nature* **1999**,*402*, 787.
49. Starke, K.; Kaduvela, A. P.; Liu, Y.; Johnson, P. D.; Van Hove, M. A.; Fadley, C. S.; Chakarian, V.; Chaban, E. E.; Meigs, G.; Chen, C. T. *Phys. Rev. B* **1996**, *53*, R10544.
50. Heinzmann, U.; Schonhense, G.; Kessler, J. *Phys. Rev. Lett.* **1979**, *42*, 1603.
51. Schonhense, G.; Ayers, A.; Friess, U.; Schafers, F.; Heinzmann, U. *Phys. Rev. Lett.* **1985**, *54*, 547.
52. Ivchenko, E. L.; Pikus, G. E. *Superlattices and Other Heterostructures. Symmetry and Optical Phenomena*; Springer: Berlin, Germany, 1997.
53. Prinz, G. A. *Phys. Today* **1995**, *48* 58.
54. Borovkov, V. V.; Hembury, G. A.; Inoue, Y. *Acc. Chem. Res.* **2004**, *37*, 449.
55. Gibbs, E. J.; Tinoco, I., Jr.; Maestre, M.; Ellinas, P. A.; Pasternack, R. F. *Biochem. Biophys. Res. Commun.***1988**, *157*, 350.
56. Gibbs, E. J.; Maurer, M. C.; Zhang, J. H.; Reiff, W. M.; Hill, D. T.; Malicka-Blaszkiewicz, M.; McKinnie, R. E.; Liu, H. Q.; Pasternack, R. F. J. *Inorg. Biochem.* **1988**, *32*, 39.
57. Pasternack, R. F.; Brigandi, R. A.; Abrams, M. J.; Williams, A. P.; Gibbs, E. J. *Inorg. Chem.* **1990**, *29*, 4483.
58. Wang, M.; Silva, G. L.; Armitage, B. A. *J. Am. Chem. Soc.* **2000**, *122*, 9977.
59. Hirschberg, J. H. K. K.; Brunsveld, L.; Ramzi, A.; Vekemans, J. A. J. M.; Sijbesma, R. P.; Meijer, E. W.*Nature* **2000**, *407*, 167.
60. Matsui, H.; Kushi, S.; Matsumoto, S.; Akazome, M.; Ogura, K. *Bull. Chem. Soc. Jpn.* **2000**, *73*, 991.
61. Musigmann, K.; Blum, K.; Thompson, D. G. *J. Phys. B*: *At. Mol. Opt. Phys.* **2001**, *34*, 2679.
62. Musigmann, M.; Bussalla, A.; Blum, K.; Thompson, D. G. *J. Phys. B*: *At. Mol. Opt. Phys.* **1999**, 4117.
63. Campbell, D. M.; Farago, P. S. *J. Phys. B* **1987**, *21*, 5133.
64. Rich, A.; Van House, J.; Hegstrom, R. A. *Phys. Rev. Lett.* **1982**, *4*8, 1341.